Macromolecules

pubs.acs.org/Macromolecules Article

Gas Transport in a Polymer of Intrinsic Microporosity (PIM-1) Substituted with Pseudo-Ionic Liquid Tetrazole-Type Structures

Michael D. Guiver,*,# Mohamed Yahia,# Mauro M. Dal-Cin, Gilles P. Robertson, Sadaf Saeedi Garakani, Naiying Du,* and Naser Tavajohi*

Cite This: *Macromolecules* 2020, 53, 8951−8959

Read Online

ACCESS | Metrics & More | Article Recommendations

ABSTRACT: We report a side group modification strategy to tailor the structure of a polymer of intrinsic microporosity (PIM-1). PIM-1 with an average of ∼50% of the repeat units converted to tetrazole is prepared, and a subsequent reaction then introduces three types of pseudo-ionic liquid tetrazole-like structures (PIM-1-IL*x*). The presence of pseudo-ionic liquid functional groups in the PIM-1 structure increases gas selectivities for O_2/N_2 and CO_2/N_2, while it decreases pure-gas permeabilities. The overall gas separation performance of PIM-1-IL*x* is close to the 2008 Robeson upper bound. Since the tetrazoles are versatile groups for building a wide variety of ionic liquids, the modification method can be expanded to explore a broad spectrum of functional groups.

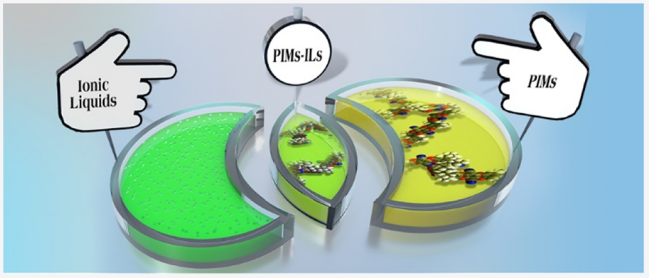

1. INTRODUCTION

Polymeric materials development with a specific functionality for gas separation membranes has become a productive field of research. Several approaches have been developed that enable fine-tuning of microporosity to overcome the gas permeability/selectivity trade-off and permeability decline caused by physical aging.

One of the most effective approaches for engineering polymer structures is the use of rigid, contorted molecular backbones that are unable to pack efficiently. The first generation of polymers of intrinsic microporosity, PIM-1, was introduced in 2004,[1−9] and the second generation, Tröger's base polymer, was introduced in 2013.[10−12] Using this method, a significant improvement in the performance of polyimides has been reported (PIM-PIs).[13−16] Another approach to disrupt polymer chain packing and increase fractional free volume further (increased permeability) is by incorporating bulky or rigid structures in the polymer repeat unit. Extensive studies have been done to improve the gas transport performance of PIM membranes using this strategy.[17] For instance, polymers with spirobifluorene units[2,3,9] and triptycene-modified Tröger's base PIMs have been reported.[10,18−23] The rigidity of the backbone and the presence of pendant groups are crucial points in this strategy. Optimum microstructures resulting from this approach depend on how the building blocks (monomers) fit together.[24] A third design approach for fine-tailoring of chain packing is by changing the linkage geometry in a similar polymer (i.e., ortho, para, or meta).[25,26] A modification of this approach is based on the thermal rearrangement of polymer chains. Thermally rearranged (TR) polymers have gained much attention during the past years as a promising strategy for producing high-performance membranes.[27−32] Details of the TR process are discussed in two reviews.[32,33] A fourth strategy for synthesizing polymers with outstanding membrane gas transport performance is by two-dimensional, ribbon-like polymer structures.[34−36] Rigidity and intrinsic free volume are crucial elements for successful design in this strategy.[24]

Another interesting alternative for tailoring microstructure is polymer side group modification. The presence of a bulky side group frustrates chain packing and increases fractional free volume (high permeability), while the nature of the side group may determine gas pair selectivity.[24] This approach has often been used with rigid backbones and resulted in ultra-microporosity in the solid state.[37,38] In particular, Smith et al. introduced an innovative rigid side group on a flexible backbone.[39]

Ionic liquids have been explored and utilized as alternative membrane materials for CO_2 membrane separations due to their high CO_2 sorption capacity.[40−44] In previous work, promising CO_2 separation performance of ionic liquids (ILs), with high permeabilities, solubilities, and diffusivities, was already demonstrated in supported ionic liquid membranes

Received: June 5, 2020
Revised: September 23, 2020
Published: October 6, 2020

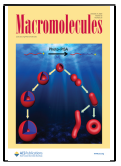

https://dx.doi.org/10.1021/acs.macromol.0c01321
Macromolecules 2020, 53, 8951−8959

Scheme 1. Synthesis of (a) PIM-1, (b) TZPIM-50, and (c) PIM-1-ILs

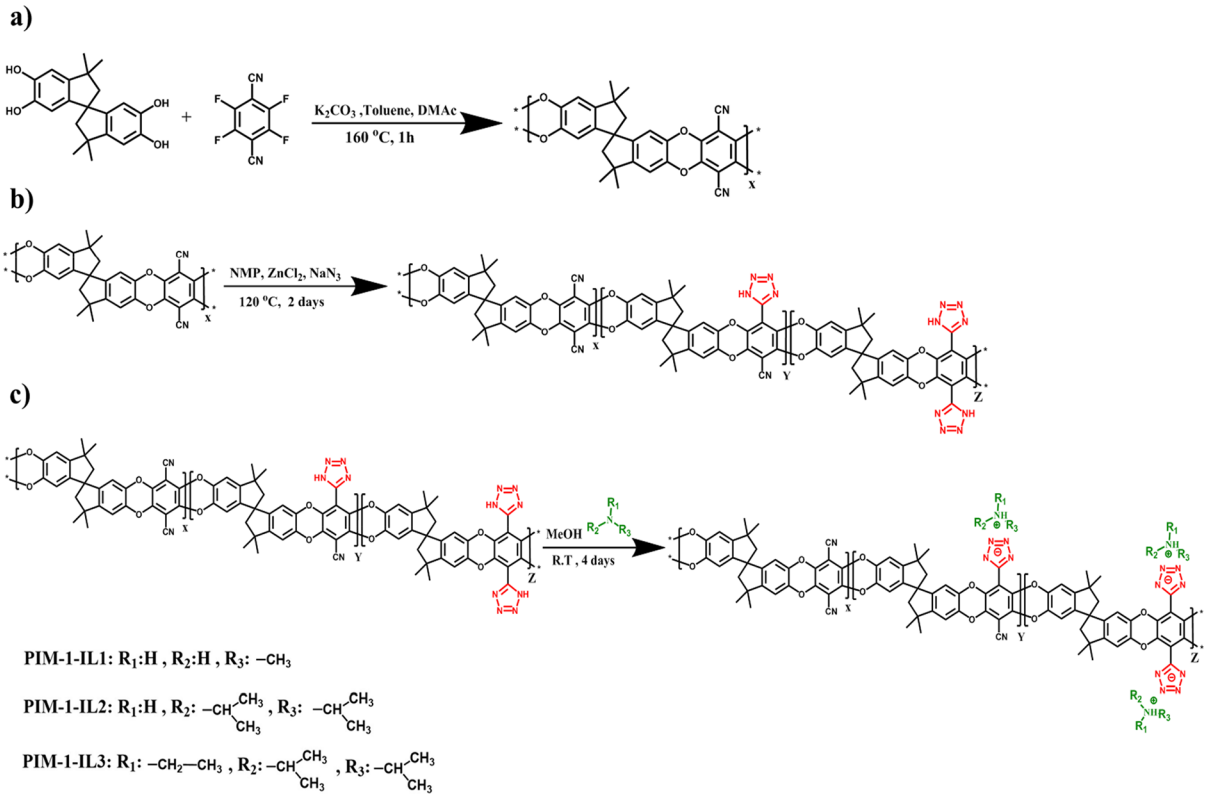

(SILMs).[45−48] However, the main drawbacks of SILMs have become apparent. Since ionic liquids are held within the pores of the support structure via relatively weak capillary forces, they are easily susceptible to being pushed through the support and result in severely compromising the membrane selectivity, if the transmembrane pressure differential exceeds the capillary forces.[49] Therefore, SILMs can usually only be operated at low pressure differentials of ∼0.2 atm. The design and optimization of porous supports have partly overcome some of these limitations, and in some instances, ILs sorbed in these supports have been reported to be stable at pressures of up to 7 atm.[47] Polymeric ionic liquids are alternative systems, which may provide improved stability and CO_2 transport.[49−51] It has been observed that polymeric ILs have a higher and faster absorption capacity for CO_2 than room temperature ionic liquids.[42,50,52] However, the polymer chains selected were inappropriate for high CO_2 permeability, resulting in poor gas transport. Beyond that mentioned above, many polymeric ILs reported previously were too brittle to be used as standalone membranes.

Here, we report the incorporation of pseudo-ILs by side group modification of PIM-1. Compared with conventional polymers used in membranes, PIMs typically have high gas permeability combined with moderately good selectivity. Gas selectivity in PIMs is not mainly diffusivity dominated as in common polymeric membranes but has significant contributions from solubility, which is similar to ionic liquids. From the viewpoint of functional polymer design, the incorporation of pseudo-IL-type structures into PIMs may provide a conceptually new avenue of exploration for membrane gas separations. Initially, PIM-1 was modified using a "click chemistry" [2 + 3] cycloaddition reaction with sodium azide and zinc chloride to yield ladder polymers containing 50% tetrazole units.[53,54] Tetrazole groups are versatile groups for building a wide variety of ionic liquids through the incorporation of suitable functional groups, such as amines. Amines have already shown their utility in ILs for CO_2 capture.[55] There are few reports of ILs derived from negatively charged tetrazole with amine, and their use has been confined to solvents, catalysts, or energetic materials.[56,57] Here, we report the synthesis, characterization, and single gas transport properties of a new class of polymers with tetrazole-based pseudo-ionic liquids (PIM-1-ILs).

2. EXPERIMENTAL SECTION

2.1. Materials. The monomers (i.e., 5,5′,6,6′-tetrahydroxy-3,3,3′,3′-tetramethylspirobisindane (TTSBI) and tetrafluoroterephthalonitrile (TFTPN)) were purchased and purified according to a reported procedure.[58] The solvents with a purity of >99%, salts with a purity of >99%, and amines: methylamine (40 wt % in H_2O), diisopropylamine, and *N*,*N*-diisopropylethylamine were purchased from Sigma-Aldrich and used as received. The solvent abbreviations are methanol (MeOH), tetrahydrofuran (THF), dimethyl sulfoxide (DMSO), dimethylacetamide (DMAc), dimethylformamide (DMF), and *N*-methylpyrrolidone (NMP). KBr was purchased from VWR International, infrared spectroscopy grade.

2.2. Preparation of PIM-1. PIM-1 (M_n, 86,000 Da; PDI, 2.0) was prepared as follows, using a reported procedure.[58] The resulting PIM-1 was produced as a bright yellow spaghetti-like polymer, which was refluxed in deionized water for several hours to remove residual solvents and salts and then dried at 100 °C for 48 h in a vacuum oven.

2.3. Preparation of Tetrazole-Containing PIMs (TZPIM-50) from PIM-1 Solution. TZPIM-50 was prepared based on a previous report.[53] The equivalence ratio of nitrile groups in PIM-1 NMP solution (1−3 g in 20 mL)/NaN_3/$ZnCl_2$ was 1:4:2. (Scheme 1b) After the reaction proceeded for 2 days at 120 °C, the reaction mixture was cooled to 60 °C, and 15 mL of diluted HCl (1:10 by volume in water) was added. The mixture was kept stirring for 3−5 h, and then, the TZPIM (∼50% degree of substitution) was precipitated and washed in the same dilute HCl. After being filtered and washed

https://dx.doi.org/10.1021/acs.macromol.0c01321
Macromolecules 2020, 53, 8951−8959

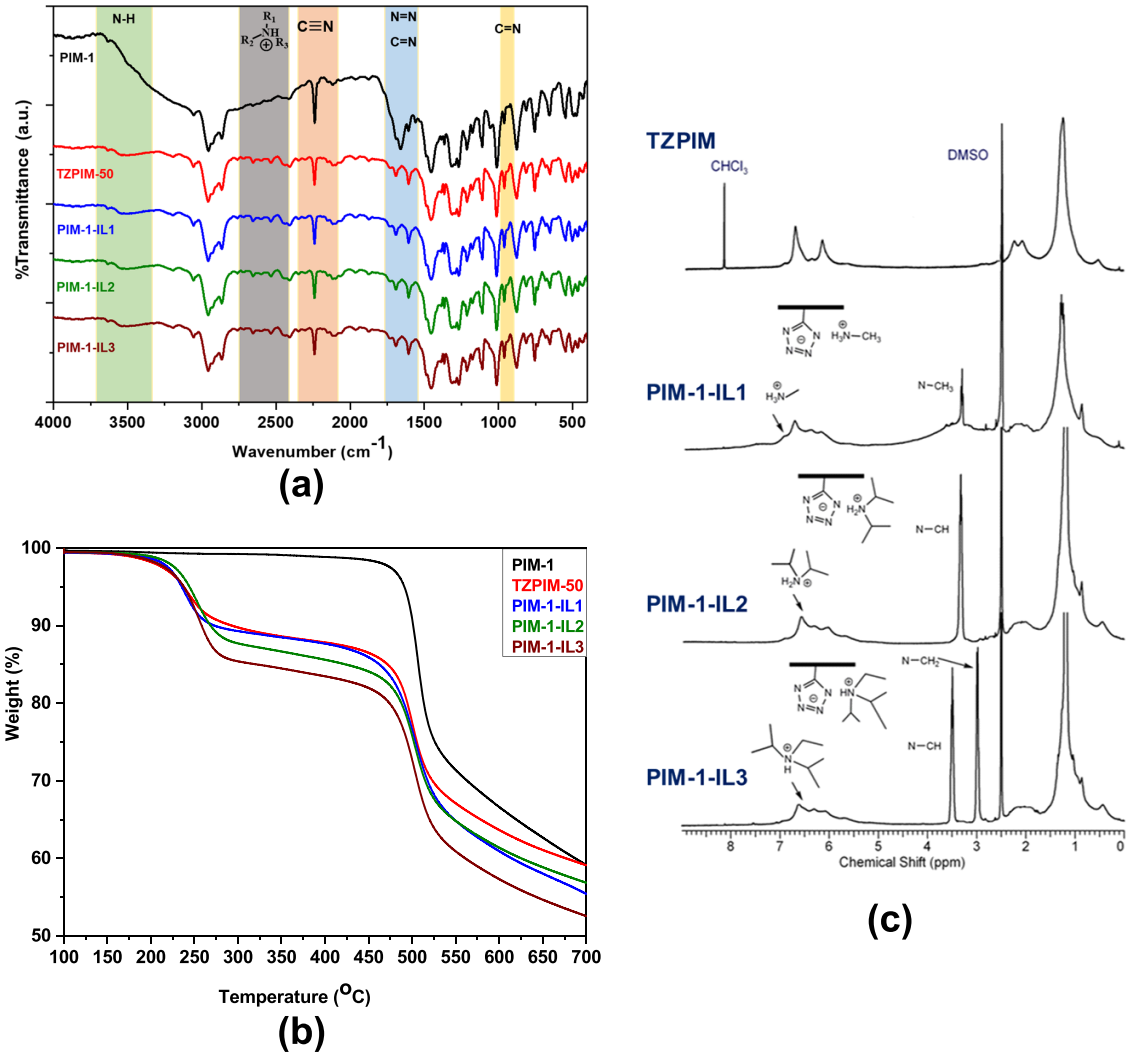

Figure 1. (a) Comparative FTIR spectra of TZPIM-50 and PIM-1-ILs. (b) TGA curves of PIM-1, TZPIM-50, PIM-1-IL1, PIM-1-IL2, and PIM-1-IL3. (c) Comparative ^{1}H NMR spectra of TZPIM-50 and PIM-1-ILs.

with water, the resulting polymer was dried in a vacuum oven at 120 °C overnight.

2.4. Preparation of PIM-1-ILs from TZPIM-50. PIM-1-ILs were synthesized from TZPIM-50. In TZPIM-50, 50% nitrile groups in PIM-1 were converted into tetrazole groups. TZPIM50 (5 mmol) with different amines in methanol solutions (15 mmol amines in 50 mL MeOH) was reacted at reflux temperature for 5−6 h, and then, the polymers were reprecipitated into water and washed with water (Scheme 1c). The polymers were dried at 80 °C in a vacuum oven for 2 days.

2.5. Characterization Methods. The structural characterization of polymers was accomplished using proton nuclear magnetic resonance (NMR) spectroscopy. Proton NMR spectra were obtained on a Varian Unity Inova spectrometer (400 MHz). The NMR solvents were $CDCl_3$ or DMSO-d_6. ^{1}H spectra were obtained by using a 5 mm pulsed field gradient indirect detection probe, and the internal references used the solvent signals $CDCl_3$ ^{1}H 7.25 ppm and DMSO-d_6 ^{1}H 2.50 ppm.

Infrared spectra (FTIR) were obtained using a Bruker IFS 66V/S instrument under vacuum conditions of 4 mbar. Dried samples (5−10 mg) were mixed with potassium bromide and manually ground in an agate mortar to produce pressed pellets. Spectra were recorded in the range of 400−4000 cm^{-1} at 4 cm^{-1} spectral resolution and 128 scans per sample. Background spectra were collected with the same settings, using pure KBr powder.

The wide-angle X-ray diffraction spectroscopy (XRD) measurements were carried out on a Bruker AXS D8 Discover instrument equipped with a Cu Kα X-ray source and scintillator point detector. The samples, which were in a powder form, were scanned in the 5−40° 2θ range, with an increment of 0.04° and at a scan speed of 8 s per point.

TGA was conducted using a Mettler Toledo TGA 3+ STAR System instrument. TGA samples were pretreated at 100 °C for 1 h under a N_2 atmosphere to remove adsorbed water. The degradation curves were obtained under a N_2 atmosphere with a heating rate of 10 °C/min to a maximum instrument temperature of 700 °C.

Gas permeability measurements were conducted on dense membranes. These were prepared from 1−2 wt % PIM solutions in $CHCl_3$ or NMP. Polymer solutions were prefiltered using 0.45 μm polypropylene syringe filters. The membranes were prepared by casting on glass or Teflon Petri dishes. The casting solvents were allowed to evaporate slowly in a glovebox at room temperature (for $CHCl_3$) or at 80 °C (for NMP) over a period of one day. The recovered membranes were immersed in boiling water for several hours. After drying under ambient conditions, they were further dried in a vacuum oven at 120 °C for one day. The thickness of the resulting membranes was in the range of 70−90 μm. The membranes PIM-1 (bright yellow) and PIM-1-ILs (brownish yellow) were flexible.

A Micromeritics TriStar 3000 porosimeter was used to measure N_2 physisorption. Adsorption−desorption isotherms were recorded at

https://dx.doi.org/10.1021/acs.macromol.0c01321
Macromolecules 2020, 53, 8951−8959

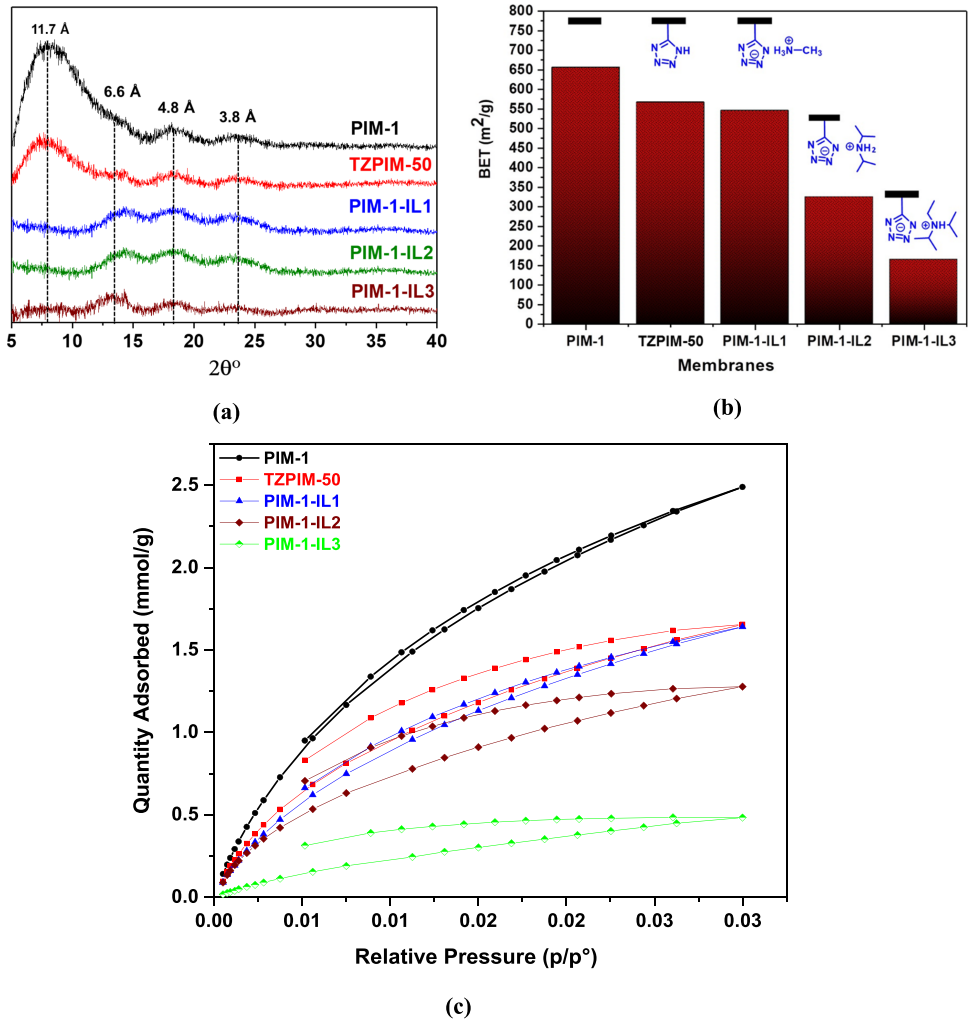

Figure 2. (a) Comparative XRD spectra. (b) BET values for PIM-1, TZPIM-50, and PIM-1 ILs. (c) BET CO_2 adsorption and desorption profiles for PIM-1, TZPIM-50, and PIM-1-IL membranes at 273 K in the low pressure range.

−196 °C after the samples, which were in a powder form, were outgassed. The specific surface areas of polymers were calculated based on the Brunauer−Emmett−Teller (BET) equation.

2.6. Gas Permeation Tests. Gas permeation tests were performed following procedures described in previous reports.[58] In order to obtain the permeability (P) in barrer, the flow rate has to be calculated in cm^3/s and the pressure measured in cmHg using the following equation

$$P\ (\text{barrers}^*) = 10^{-10} \times \frac{273.15\ (\text{K})}{T\ (\text{K})} \times \frac{l\ (\text{cm})}{\Delta P\ (\text{cmHg}) \times A\ (\text{cm}^2)} \times \frac{dV\ (\text{cm}^3)}{dt\ (\text{s})}$$

where dV/dt is the permeate-side flow rate, and T is the operating temperature (K). A is the membrane effective area, which was 0.78 cm^2.

3. RESULTS AND DISCUSSION

An absorption band at 2240 cm^{-1} in the FTIR spectrum (Figure 1a) of PIM-1 corresponds to nitrile groups. The absence of an N−H group is given by the lack of absorption bands in the range of 3000−3600 cm^{-1}. The absorption bands and their corresponding intensities in TZPIM-50, PIM-1-IL1, PIM-1-IL2, and PIM-1-IL3 exhibit similarities. In the tetrazole-substituted polymers, the nitrile absorption band intensities decreased to ∼50% compared with PIM-1. Broad absorption bands in the range of 3250−3600 cm^{-1}, indicative of N−H stretching associated with N−H···N hydrogen bonding were observed. Absorption bands corresponding to quaternary nitrogen vibrations were in the range of 2300−2800 cm^{-1}.[59] The stretching vibrations of the N═N and N−H groups were observed as an intense sharp absorption near 1650 cm^{-1}, which suggests that a portion of the nitrile groups were converted into tetrazole groups.[60] Small new bands associated with the tetrazole ring appearing near 1550 cm^{-1} are characteristic of C═N stretching,[61] while bending vibrations at 950 cm^{-1} are characteristic of the tetrazole ring. Furthermore, the absorption band at 950 cm^{-1} arises from −C−H bending vibration of aromatic alkenes. The absorption band around 1550−1660 cm^{-1} is from the conjugated alkene (C═C) [phenyl−CN, electron withdrawing; −phenyl, electron donating]. The bands above 3000 cm^{-1} are due to unsaturated −C═C−H stretch.

PIM-1, TZPIM-50, and the PIM-1-ILs were further characterized by TGA, and the comparative results are shown in Figure 1b. No observed degradation of PIM-1 occurred before 450 °C at a heating rate of 10 °C/min in N_2. Usually, nitrile-containing polymers, such as PIM-1, have high thermal stability, which is likely due to strong dipolar interactions.[62] It is observed that TZPIM-50 and PIM-1-ILs

https://dx.doi.org/10.1021/acs.macromol.0c01321
Macromolecules 2020, 53, 8951−8959

decompose thermally in three stages: the first two stages proceed with the degradation of the tetrazole ring (around 225−450 °C), while the final stage corresponds to the polymeric residue thermo-oxidative degradation at ∼700 °C. As reported by Prokudin et al.,[63] decomposition between 225 and 450 °C can be attributed to the extrusion of N_2 from the decomposition of tetrazole groups.

As shown in Figure 1b, the initial stage weight losses (i.e., before 225 °C) for TZPIM-50, PIM-1-IL1, PIM-1-IL2, and PIM-1-IL3 are 8.90, 10.30, 11.07, and 13.43%, respectively, while the weight losses at the second stage (i.e., before 450 °C) are 13.54, 14.22, 15.9, and 17.98%, respectively. This indicates that the initial two-stage weight losses for PIM-1-ILs correspond to the complete decomposition of tetrazole, which provides further supporting evidence for the presence of tetrazole structures on the main chain.

The weight losses at the last stage of decomposition (before 700 °C) for TZPIM-50, PIM-1-IL1, PIM-1-IL2, and PIM-1-IL3 are 40.57, 44.61, 43.04, and 47.48%, respectively. The late-stage decomposition is close to 50% of the complete decomposition of PIM-1-ILs, which indicates that the residue of all polymer main chains had similar structures.

In summary, the PIM-1 is thermally more stable than TZPIM-50 and PIM-1-ILs. However, all PIM-1-ILs still show sufficiently high thermal stability for the gas separation membranes, even after the nitrile groups are converted to tetrazole groups by the [2 + 3] cycloaddition reaction and modification of tetrazole structures with different ionic liquids.

The ^{1}H NMR spectra (Figure 1c) support the structures of these PIM-1-ILs. The ^{1}H NMR signal intensities and signal shapes of these polymers were observed at 100 °C NMR probe temperatures. As expected from the molecular structure, the detected signal intensity ratio of the aromatic (6.2−6.8 ppm) and aliphatic (0.3−2.4 ppm, CH_2, and CH_3) regions in TZPIM-50 is exactly 4H:16H. For PIM-1-IL1, besides having similar aromatic and aliphatic regions with the same integration of 4H:16H, an additional signal arose at 3.3 ppm, which corresponds to N−CH_3 with an integration of 3H. The large polymer molecules, combined with hydrogen bonding and highly viscous DMSO-d_6 solvent, result in poor spectral quality and broad signals. Thus, the ^{1}H NMR spectra were acquired at 100 °C to improve resolution and obtain more accurate signal integration. Labile −NH proton signals are particularly susceptible to temperature and may change shape and even chemical shift, while CH protons usually remain unchanged. The signals between 6.8 and 7.2 ppm were affected by temperature changes. Hence, to confirm the −NH proton signal, a drop of D_2O was added into the NMR tube. The tube was shaken vigorously, and the spectrum was re-acquired. Since deuterium atoms readily exchange with labile protons while remaining undetected by ^{1}H NMR, the qualitative D_2O exchange resulted in the disappearance of the broad −NH proton signals results in the 6.8−7.2 ppm region, thus confirming the presence of −NH labile protons.

For PIM-1-IL2 and TZPIM-50, in comparing N−CH-$(CH_3)_2$ with −CH_2 and −CH_3 of the PIM main chain, the integration of aromatic (6.2−6.8 ppm) and aliphatic (0.3−2.4 ppm) regions is 4H:24H. The N−CH corresponds to the sharp signal at ∼3.4 ppm (m) with an integration of 2H, while −NH protons correspond to the small shoulder signal in the range of 6.8−7.2 ppm. For PIM-1-IL3, the relative integration of aromatic (6.2−6.8 ppm) versus aliphatic (0.3−2.4 ppm) protons from the PIM main chain is 4H:27H. Sharp signals are observed for N−CH_2 (2H, d, 2.9 ppm) and N−CH (2H, m, 3.5 ppm). It is noteworthy that no observable signal appeared at around 6.8−7.2 ppm, which implies that hydrogen bonded −NH protons are absent.

XRD measurements were performed to investigate chain packing (Figure 2a). The absence of a sharp diffraction peak in the XRD patterns indicates an amorphous structure for the synthesized polymers. The broad peak appearing at 3.8 Å is representative of aromatic systems,[64] and the peak at 4.8 Å indicates the *d*-spacing of efficiently packed chains. The broad peaks at 6.6 and 11.7 Å for PIM-1 are attributed to loosely packed polymer chains due to their contorted ladder architecture and the creation of micropores.[65−67] However, in comparison with TZPIM-50 and PIM-1-ILs, a peak at 6.6 Å did not have a sharp appearance owing to overlap between the 6.6 and 11.7 Å peaks.

The incorporation of the tetrazole groups into the PIM-1 structure caused a reduction in a broad peak at 2θ = 11.7°, suggesting that the *d*-spacing of TZPIM-50 membrane chains became smaller. This is in agreement with the results of the BET, presented in Figure 2b. The addition of the amines into the TZPIM-50 eliminated the broad peak at 2θ = 11.7° and slightly increased the peak at 6.6 Å. This can be attributed to the presence of the amine groups inside the micropore cavity.

The BET surface area of the PIM-1 membrane is higher than those of TZPIM-50 and PIM-1-ILs, which indicates that the overall PIM-1 porosity is higher than those of TZPIM-50 and PIM-ILs. This is because tetrazole and different pseudo-ionic liquid structures diminish the size of micropore cavities and interchain distance, by space filling and interchain interactions, which further rigidify the polymer chains. Although both tetrazole and ionic liquid groups partially occupy the micropores, these reductions are higher in PIM-1-ILs, and the surface area decreased as the IL size increased. It will be shown that the permselectivity improved for PIM-1-IL membranes, when compared with TZPIM-50 and PIM-1 membranes. The reductions of surface area were well-correlated with the permeability and selectivity for PIM-1, TZPIM-50, and PIM-IL membranes.

The adsorption capacity of CO_2 for PIM-1 is higher than those for TZPIM-50 and PIM-1-ILs, presented in Figure 2c. Based on these BET results, it appears that the increase in permselectivity of PIM-1-ILs can be attributed to the enhancement of diffusion selectivity rather than the affinity between the pseudo-ionic liquid and CO_2.

One of the crucial parameters for the processability of the synthesized PIMs is the solubility in organic solvents. Table 1

Table 1. Solubility of PIM-1, TZPIM-50, and PIM-1-ILs[a]

	polymers				
solvent	PIM-1	TZPIM-50	PIM-1-IL1	PIM-1-IL2	PIM-1-IL3
THF	++	-	-	-	-
CH_2Cl_2	++	-	-	-	-
$CHCl_3$	++	+	-	-	-
DMAc	-	++	++	++	++
NMP	+	++	++	++	++
DMF	-	+	+	+	+
DMSO	-	+	+	+	+
methanol	-	-	-	-	-

[a]Key: ++, readily soluble; +, soluble with heating; +-, partially soluble; -, insoluble.

https://dx.doi.org/10.1021/acs.macromol.0c01321
Macromolecules 2020, 53, 8951−8959

lists the solubility data of the polymers. PIM-1 is readily soluble in THF, CH_2Cl_2, and $CHCl_3$, soluble by heating in NMP but insoluble in polar aprotic solvents such as DMF, DMAc, and DMSO. Different from PIM-1, TZPIM-50 is readily soluble in DMAc and NMP and soluble in DMF, DMSO and $CHCl_3$ with heating but insoluble in THF and CH_2Cl_2. The solubility of all the PIM-1-ILs is similar to that of TZPIM-50, but they are insoluble in $CHCl_3$, even with heating. When comparing TZPIM-50 and all three PIM-ILs, gels formed more readily for DMF solutions of TZPIM-50 and primary amine (PIM-1-IL1) due to strong hydrogen bonding, while PIM-1-IL3 exhibited the least gel formation. It was visually observed that the degree of swelling of the polymer membranes in chloroform increased in the order of PIM-1-IL1 < PIM-1-IL2 < PIM-1-IL3, while in methanol, they increased in the order of PIM-1-IL3 < PIM-1-IL2 < PIM-1-IL1. These interesting observations also indicate that the solubility of these polymers was affected by the different amine cations of the tetrazole pseudo-ionic liquids.

A summary of single gas permeability and ideal selectivity values for various gas pairs is shown in Table 2. It is known

Table 2. Gas Permeabilities and Ideal Selectivities of PIM-1, TZPIM-50, PIM-1-IL1, PIM-1-IL2, and PIM-1-IL3

	P (barrer[a])			α[b]	
polymers	O_2	N_2	CO_2	O_2/N_2	CO_2/N_2
PIM-1-H_2O	1113	398	5500	2.9	13.8
PIM-1-MeOH	1545	486	7340	3.2	15.1
TZPIM-50-H_2O	276	129	1576	2.1	12.2
TZPIM-50-MeOH	752	192	5070	3.9	26.4
PIM-1-IL1	169	36	1043	4.7	29
PIM-1-IL2	151	35	1010	4.3	29
PIM-1-IL3	102	23	817	4.5	35.5

[a]Permeability coefficients measured at 25 °C and 100 psig (6.89 bar) feed pressure. 1 barrer = 10^{-10} [cm^3 (STP)·cm]/(cm^2·s·cmHg). [b]Ideal selectivity $\alpha = (P_a)/(P_b)$.

that the gas permeability and selectivity of PIM-1 are largely affected by pretreatment and membrane fabrication conditions and are especially sensitive to moisture.[7] Variations in the permeability of PIM-1 between previously reported data and the present data are shown in Figures 3 and 4.

The post-treatment protocol for PIM membranes is normally methanol, which is conducted to remove film forming history and residual solvents. However, methanol is unsuitable for PIM-1-IL pretreatment because of a propensity for swelling. In place of methanol, PIM-1-IL membranes were treated solely in boiling water, which was slightly acidified with HCl to pH 5, to remove residual polar aprotic casting solvent and salts. After being dried under ambient conditions, the membranes were dehydrated in a vacuum oven for at least 24 h by gradually increasing the temperature from room temperature to 120 °C. For comparison, the PIM-1 membrane was treated in a similar manner. Consequently, it is important to note that the gas transport properties of PIM-1 differ substantially from commonly reported literature values, which relate to differences in the water versus methanol post-treatment. Figure 3 shows that the O_2/N_2 selectivities for PIM-1 and PIM-ILs lie between the 1991 and 2008 Robeson upper bounds. The substitution of pseudo-ionic liquid pendant groups in the PIM-1 structure increases the selectivity of PIM-1-IL1, PIM-1-IL2, and PIM-1-IL3 up to 65, 50, and 58%,

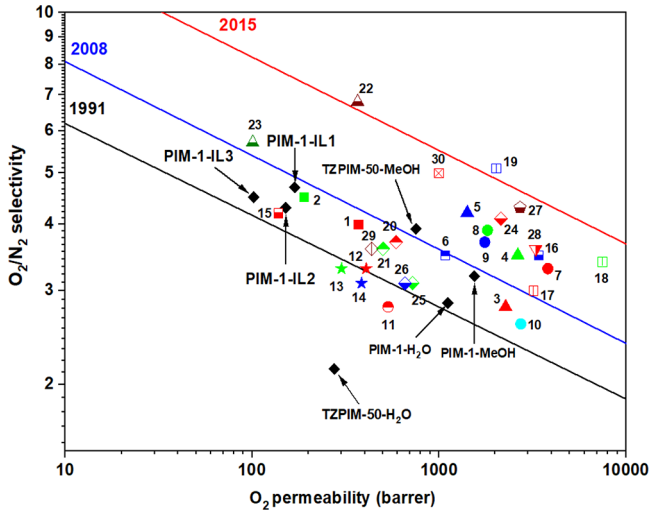

Figure 3. Relationship between O_2/N_2 selectivity and O_2 permeability. PIM-1-IL1, PIM 1-IL2, PIM-1-IL3, and PIM-1 are labeled in black color. Other PIM polymers are labeled as follows: (1) PIM-1a,[3] (2) PIM-7a,[3] (3) PIM-1b (128 μm),[17] (4) spirobifluorene-PIM-1b (SBF-PIM-1b) (180 μm),[17] (5) spirobifluorene-PIM-1b (SBF-PIM-1b) (80 μm),[17] (6) PIM-1c (102 μm),[68] (7) spirobifluorene-PIM-2b (SBF-PIM-2b) (115 μm),[69] (8) spirobifluorene-PIM-3b (SBF-PIM-3b) (120 μm),[69] (9) spirobifluorene-PIM-4b (SBF-PIM-4b) (120 μm),[69] (10) spirobifluorene-PIM-5b (SBF-PIM-5b) (98 μm),[69] (11) PIM-hexaphenylbenzene-b (PIM-HPB-b),[70] (12) PIM-methyl-hexaphenylbenzene-b (PIM-CH_3-HPB-b),[71] (13) PIM-bromo-hexaphenylbenzene-b PIM-Br-HPB-b,[71] (14) PIM-cyano-hexaphenylbenzene-b (PIM-CN-HPB-b),[71] (15) tetraphenylethylene-PIM-c (TPE-PIM-c),[72] (16) PIM-C1-d,[73] (17) PIM-tetramethyltetrahydronaphthalene-spirobisindane-b (PIM-TMN-SBI-b) (166 μm),[34] (18) PIM-tetramethyltetrahydronaphthalene-triptycene-b (PIM-TMN-Trip-b) (195 μm),[34] (19) PIM-tetramethyltetrahydronaphthalene-triptycene-Tröger base-b (PIM-TMN-Trip-TB-b),[34] (20) PIM-7c,[74] (21) phenazine spirobisindane AB-type-c (PSBI-AB-c),[74] (22) triptycene PIM-1f (TPIM-1f),[35] (23) triptycene PIM-2f (TPIM-2f),[35] (24) PIM-ethanoanthracene-Tröger base-b (PIM-EA-TB-b) (181 μm),[10] (25) PIM-spirobisindane-Tröger base-b (PIM-SBI-TB-b) (157 μm),[10] (26) PIM-spirobisindane-Tröger base-b (PIM-SBI-TB-b) (128 μm),[10] (27) PIM-triptycene-Tröger base-b (PIM-Trip-TB-b) (132 μm),[19] (28) PIM-benzotriptycene-Tröger base-b (PIM-BTrip-TB-b) (180 mm),[21] (29) Tröger base-adamantane-methyl-b (TB-Ad-Me-b) (125 μm),[75] and (30) PIM-methanopentacene-Tröger base-b (PIM-MP-TB-b) (94 μm).[76] Upper bounds are represented by the black line (1991),[77] blue line (2008),[78] and red line (2015).[79,80]

respectively, relative to PIM-1, with concomitant decreases in O_2 permeability approximately following the trade-off limits. The substituent resides in the PIM-1 cavities and decreases the overall microporosity, particularly for the sterically largest substituent. Compared with PIM-1, PIM-1-ILs generally exhibit lower oxygen permeabilities but higher O_2/N_2 selectivities, with performance trending closer to the 2008 Robeson upper bound.

PIM-1-ILs show good CO_2/N_2 transport performance, as shown in Figure 4, placing them close to the 2008 Robeson upper bound.[78] The interchain distance of the PIM-1-ILs does not appear to be significantly changed with respect to PIM-1 by introducing pseudo-IL groups since they appear to occupy the interchain space. The sterically larger amine counterions have lower gas permeabilities (see Table 1), suggesting that the pseudo-ILs act more as interchain filling materials within the PIM structures. Thus, modifying the cations or anions in the

https://dx.doi.org/10.1021/acs.macromol.0c01321
Macromolecules 2020, 53, 8951−8959

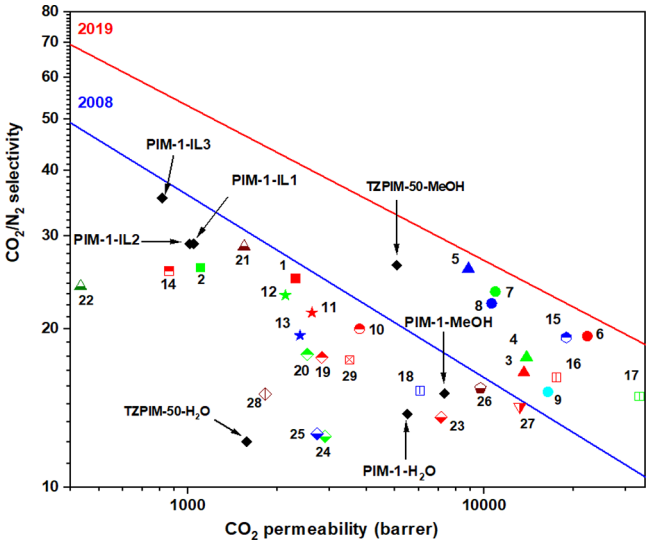

Figure 4. Relationship between CO_2 permeability and CO_2/N_2 selectivity. PIM-1, PIM-1-IL1, PIM 1-IL2, and PIM-1-IL3 are labeled in black color. Other PIM polymers are labeled as follows: (1) PIM-1a,[3] (2) PIM-7a,[3] (3) PIM-1b (128 μm),[17] (4) spirobifluorene-PIM-1b (SBF-PIM-1b) (180 μm),[17] (5) spirobifluorene-PIM-1b (SBF-PIM-1b) (80 μm),[17] (6) spirobifluorene-PIM-2b (SBF-PIM-2b) (115 μm),[69] (7) spirobifluorene-PIM-3b (SBF-PIM-3b) (120 μm),[69] (8) spirobifluorene-PIM-4b (SBF-PIM-4b) (120 μm),[69] (9) spirobifluorene-PIM-5b (SBF-PIM-5b) (98 μm),[69] (10) PIM-hexaphenylbenzene-b (PIM-HPB-b),[70] (11) PIM-methyl-hexaphenylbenzene-b (PIM-CH_3-HPB-b),[71] (12) PIM-bromo-hexaphenylbenzene-b PIM-Br-HPB-b,[71] (13) PIM-cyano-hexaphenylbenzene-b (PIM-CN-HPB-b),[71] (14) tetraphenylethylene-PIM-c (TPE-PIM-c),[72] (15) PIM-C1-d,[73] (16) PIM-tetramethyltetrahydronaphthalene-spirobisindane-b (PIM-TMN-SBI-b) (166 μm),[34] (17) PIM-tetramethyltetrahydronaphthalene-triptycene-b (PIM-TMN-Trip-b) (195 μm),[34] (18) PIM-tetramethyltetrahydronaphthalene-triptycene-Tröger base-b (PIM-TMN-Trip-TB-b),[34] (19) PIM-7c,[74] (20) phenazine spirobisindane AB-type-c (PSBI-AB-c),[74] (21) triptycene PIM-1f (TPIM-1f),[35] (22) triptycene PIM-2f (TPIM-2f),[35] (23) PIM-ethanoanthracene-Tröger base-b (PIM-EA-TB-b) (181 μm),[10] (24) PIM-spirobisindane-Tröger base-b (PIM-SBI-TB-b) (157 μm),[10] (25) PIM-spirobisindane-Tröger base-b (PIM-SBI-TB-b) (128 μm),[10] (26) PIM-triptycene-Tröger base-b (PIM-Trip-TB-b) (132 μm),[19] (27) PIM-benzotriptycene-Tröger base-b (PIM-BTrip-TB-b) (180 μm),[21] (28) Tröger base-adamantane-methyl-b (TB-Ad-Me-b) (125 μm),[75] and (29) PIM-methanopentacene-Tröger base-b (PIM-MP-TB-b) (94 μm).[76] Upper bounds are represented by the blue line (2008)[78] and the red line (2019).[80]

PIMs is a conceptually simple approach to tune gas selectivity and permeability.

4. CONCLUSION

A conceptually new approach to novel-structured polymers of intrinsic microporosity containing pseudo-ionic liquids (PIM-1-ILs) is presented, whereby tetrazole-modified PIM-1 with a degree of tetrazole substitution of ~50% was reacted with various amines to form ionic sites. Compared with PIM-1, the PIM-1-ILs exhibit overall attractive gas transport properties. Higher gas selectivity than that of PIM-1 is achieved, while the overall performance is close to the 2008 Robeson upper bound for the O_2/N_2 and CO_2/N_2 gas pairs. Tetrazole groups are versatile groups for building a wide variety of ionic liquids through the incorporation of suitable functional groups, such as amines. We envisage that the gas transport properties of these PIM-1-ILs can be readily tuned by selecting different cations for TZPIMs, or the concept can be extended to other ionic structures, beyond using tetrazole.

AUTHOR INFORMATION

Corresponding Authors

Michael D. Guiver − *State Key Laboratory of Engines, Tianjin University, Tianjin 300072, P.R. China; Collaborative Innovation Center of Chemical Science and Engineering (Tianjin), Tianjin 300072, P.R. China;* orcid.org/0000-0003-2619-6809; Email: michael.guiver@outlook.com

Naiying Du − *National Research Council Canada, Ottawa, Ontario K1A 0R6, Canada*; Email: naiying.du@nrc-cnrc.gc.ca

Naser Tavajohi − *Department of Chemistry, Umeå University, Umeå SE-901 87, Sweden;* orcid.org/0000-0002-3973-0938; Email: naser.tavajohi@outlook.com

Authors

Mohamed Yahia − *Department of Chemistry, Umeå University, Umeå SE-901 87, Sweden*

Mauro M. Dal-Cin − *National Research Council Canada, Ottawa, Ontario K1A 0R6, Canada*

Gilles P. Robertson − *National Research Council Canada, Ottawa, Ontario K1A 0R6, Canada*

Sadaf Saeedi Garakani − *Department of Materials and Environmental Chemistry, Stockholm University, SE-10691 Stockholm, Sweden*

Complete contact information is available at: https://pubs.acs.org/10.1021/acs.macromol.0c01321

Author Contributions

#M.D.G. and M.Y. contributed equally.

Notes

The authors declare no competing financial interest.

ACKNOWLEDGMENTS

This work was partly supported by the State Key Laboratory of Engines and the Natural Resources Canada Clean Energy Fund. We appreciate the financial support from the Kempe Foundation and Bio4energy program.

REFERENCES

(1) Budd, P. M.; Elabas, E. S.; Ghanem, B. S.; Makhseed, S.; McKeown, N. B.; Msayib, K. J.; Tattershall, C. E.; Wang, D. Solution-Processed, Organophilic Membrane Derived from a Polymer of Intrinsic Microporosity. *Adv. Mater.* **2004**, *16*, 456−459.

(2) Budd, P. M.; Ghanem, B. S.; Makhseed, S.; McKeown, N. B.; Msayib, K. J.; Tattershall, C. E. Polymers of intrinsic microporosity (PIMs): robust, solution-processable, organic nanoporous materials. *Chem. Commun.* **2004**, *2*, 230−231.

(3) Budd, P. M.; McKeown, N. B.; Fritsch, D. Free volume and intrinsic microporosity in polymers. *J. Mater. Chem.* **2005**, *15*, 1977−1986.

(4) Budd, P. M.; Msayib, K. J.; Tattershall, C. E.; Ghanem, B. S.; Reynolds, K. J.; McKeown, N. B.; Fritsch, D. Gas separation membranes from polymers of intrinsic microporosity. *J. Membr. Sci.* **2005**, *251*, 263−269.

(5) McKeown, N. B.; Budd, P. M.; Msayib, K. J.; Ghanem, B. S.; Kingston, H. J.; Tattershall, C. E.; Makhseed, S.; Reynolds, K. J.; Fritsch, D. Polymers of Intrinsic Microporosity (PIMs): Bridging the Void between Microporous and Polymeric Materials. *Chemistry−A European Journal* **2005**, *11*, 2610−2620.

https://dx.doi.org/10.1021/acs.macromol.0c01321
Macromolecules 2020, 53, 8951−8959

(6) Li, P.; Chung, T. S.; Paul, D. R. Gas sorption and permeation in PIM-1. *J. Membr. Sci.* **2013**, *432*, 50−57.
(7) Budd, P. M.; McKeown, N. B.; Ghanem, B. S.; Msayib, K. J.; Fritsch, D.; Starannikova, L.; Belov, N.; Sanfirova, O.; Yampolskii, Y.; Shantarovich, V. Gas permeation parameters and other physicochemical properties of a polymer of intrinsic microporosity: Polybenzodioxane PIM-1. *J. Membr. Sci.* **2008**, *325*, 851−860.
(8) Gemeda, A. E.; De Angelis, M. G.; Du, N.; Li, N.; Guiver, M. D.; Sarti, G. C. Mixed gas sorption in glassy polymeric membranes. III. CO_2/CH_4 mixtures in a polymer of intrinsic microporosity (PIM-1): Effect of temperature. *J. Membr. Sci.* **2017**, *524*, 746−757.
(9) Thomas, S.; Pinnau, I.; Du, N.; Guiver, M. D. Pure- and mixed-gas permeation properties of a microporous spirobisindane-based ladder polymer (PIM-1). *J. Membr. Sci.* **2009**, *333*, 125−131.
(10) Carta, M.; Malpass-Evans, R.; Croad, M.; Rogan, Y.; Jansen, J. C.; Bernardo, P.; Bazzarelli, F.; McKeown, N. B. An Efficient Polymer Molecular Sieve for Membrane Gas Separations. *Science* **2013**, *339*, 303.
(11) Fan, Y.; Li, C.; Zhang, X.; Yang, X.; Su, X.; Ye, H.; Li, N. Tröger 's base mixed matrix membranes for gas separation incorporating NH2-MIL-53(Al) nanocrystals. *J. Membr. Sci.* **2019**, *573*, 359−369.
(12) Xiao, Y.; Zhang, L.; Xu, L.; Chung, T.-S. Molecular design of Tröger's base-based polymers with intrinsic microporosity for gas separation. *J. Membr. Sci.* **2017**, *521*, 65−72.
(13) Rogan, Y.; Malpass-Evans, R.; Carta, M.; Lee, M.; Jansen, J. C.; Bernardo, P.; Clarizia, G.; Tocci, E.; Friess, K.; Lanč, M.; McKeown, N. B. A highly permeable polyimide with enhanced selectivity for membrane gas separations. *J. Mater. Chem. A* **2014**, *2*, 4874−4877.
(14) Rogan, Y.; Starannikova, L.; Ryzhikh, V.; Yampolskii, Y.; Bernardo, P.; Bazzarelli, F.; Jansen, J. C.; McKeown, N. B. Synthesis and gas permeation properties of novel spirobisindane-based polyimides of intrinsic microporosity. *Polym. Chem.* **2013**, *4*, 3813−3820.
(15) Hossain, I.; Nam, S. Y.; Rizzuto, C.; Barbieri, G.; Tocci, E.; Kim, T.-H. PIM-polyimide multiblock copolymer-based membranes with enhanced CO_2 separation performances. *J. Membr. Sci.* **2019**, *574*, 270−281.
(16) Xu, X.; Wang, J.; Dong, J.; Li, H.-B.; Zhang, Q.; Zhao, X. Ionic polyimide membranes containing Tröger's base: Synthesis, microstructure and potential application in CO_2 separation. *J. Membr. Sci.* **2020**, *602*, 117967.
(17) Bezzu, C. G.; Carta, M.; Tonkins, A.; Jansen, J. C.; Bernardo, P.; Bazzarelli, F.; McKeown, N. B. A spirobifluorene-based polymer of intrinsic microporosity with improved performance for gas separation. *Adv. Mater.* **2012**, *24*, 5930−5933.
(18) Alghunaimi, F.; Ghanem, B.; Alaslai, N.; Swaidan, R.; Litwiller, E.; Pinnau, I. Gas permeation and physical aging properties of iptycene diamine-based microporous polyimides. *J. Membr. Sci.* **2015**, *490*, 321−327.
(19) Carta, M.; Croad, M.; Malpass-Evans, R.; Jansen, J. C.; Bernardo, P.; Clarizia, G.; Friess, K.; Lanč, M.; McKeown, N. B. Triptycene induced enhancement of membrane gas selectivity for microporous Tröger's base polymers. *Adv. Mater.* **2014**, *26*, 3526−3531.
(20) Guiver, M. D.; Lee, Y. M. Polymer rigidity improves microporous membranes. *Science* **2013**, *339*, 284−285.
(21) Rose, I.; Carta, M.; Malpass-Evans, R.; Ferrari, M.-C.; Bernardo, P.; Clarizia, G.; Jansen, J. C.; McKeown, N. B. Highly permeable benzotriptycene-based polymer of intrinsic microporosity. *ACS Macro Lett.* **2015**, *4*, 912−915.
(22) Zhang, C.; Fu, L.; Tian, Z.; Cao, B.; Li, P. Post-crosslinking of triptycene-based Tröger's base polymers with enhanced natural gas separation performance. *J. Membr. Sci.* **2018**, *556*, 277−284.
(23) Zhuang, Y.; Seong, J. G.; Do, Y. S.; Lee, W. H.; Lee, M. J.; Guiver, M. D.; Lee, Y. M. High-strength, soluble polyimide membranes incorporating Tröger's Base for gas separation. *J. Membr. Sci.* **2016**, *504*, 55−65.
(24) Corrado, T.; Guo, R. Macromolecular design strategies toward tailoring free volume in glassy polymers for high performance gas separation membranes. *Molecular Systems Design & Engineering* **2020**, *5*, 22−48.
(25) Madzarevic, Z. P.; Shahid, S.; Nijmeijer, K.; Dingemans, T. J. The role of ortho-, meta- and para-substitutions in the main-chain structure of poly(etherimide)s and the effects on CO_2/CH_4 gas separation performance. *Sep. Purif. Technol.* **2019**, *210*, 242−250.
(26) Borjigin, H.; Liu, Q.; Zhang, W.; Gaines, K.; Riffle, J. S.; Paul, D. R.; Freeman, B. D.; McGrath, J. E. Synthesis and characterization of thermally rearranged (TR) polybenzoxazoles: Influence of isomeric structure on gas transport properties. *Polymer* **2015**, *75*, 199−210.
(27) Park, H. B.; Kamcev, J.; Robeson, L. M.; Elimelech, M.; Freeman, B. D. Maximizing the right stuff: The trade-off between membrane permeability and selectivity. *Science* **2017**, *356*, eaab0530.
(28) Stevens, K. A.; Smith, Z. P.; Gleason, K. L.; Galizia, M.; Paul, D. R.; Freeman, B. D. Influence of temperature on gas solubility in thermally rearranged (TR) polymers. *J. Membr. Sci.* **2017**, *533*, 75−83.
(29) Robeson, L. M.; Dose, M. E.; Freeman, B. D.; Paul, D. R. Analysis of the transport properties of thermally rearranged (TR) polymers and polymers of intrinsic microporosity (PIM) relative to upper bound performance. *J. Membr. Sci.* **2017**, *525*, 18−24.
(30) Park, H. B.; Han, S. H.; Jung, C. H.; Lee, Y. M.; Hill, A. J. Thermally rearranged (TR) polymer membranes for CO_2 separation. *J. Membr. Sci.* **2010**, *359*, 11−24.
(31) Li, S.; Jo, H. J.; Han, S. H.; Park, C. H.; Kim, S.; Budd, P. M.; Lee, Y. M. Mechanically robust thermally rearranged (TR) polymer membranes with spirobisindane for gas separation. *J. Membr. Sci.* **2013**, *434*, 137−147.
(32) Kim, S.; Lee, Y. M. Rigid and microporous polymers for gas separation membranes. *Prog. Polym. Sci.* **2015**, *43*, 1−32.
(33) Galizia, M.; Chi, W. S.; Smith, Z. P.; Merkel, T. C.; Baker, R. W.; Freeman, B. D. 50th Anniversary Perspective: Polymers and Mixed Matrix Membranes for Gas and Vapor Separation: A Review and Prospective Opportunities. *Macromolecules* **2017**, *50*, 7809−7843.
(34) Rose, I.; Bezzu, C. G.; Carta, M.; Comesaña-Gándara, B.; Lasseuguette, E.; Ferrari, M. C.; Bernardo, P.; Clarizia, G.; Fuoco, A.; Jansen, J. C. Polymer ultrapermeability from the inefficient packing of 2D chains. *Nat. Mater.* **2017**, *16*, 932−937.
(35) Ghanem, B. S.; Swaidan, R.; Ma, X.; Litwiller, E.; Pinnau, I. Energy-Efficient Hydrogen Separation by AB-Type Ladder-Polymer Molecular Sieves. *Adv. Mater.* **2014**, *26*, 6696−6700.
(36) Yin, Y.; Guiver, M. D. Microporous polymers: ultrapermeable membranes. *Nat. Mater.* **2017**, *16*, 880−881.
(37) Luo, S.; Liu, Q.; Zhang, B.; Wiegand, J. R.; Freeman, B. D.; Guo, R. Pentiptycene-based polyimides with hierarchically controlled molecular cavity architecture for efficient membrane gas separation. *J. Membr. Sci.* **2015**, *480*, 20−30.
(38) Tsui, N. T.; Paraskos, A. J.; Torun, L.; Swager, T. M.; Thomas, E. L. Minimization of Internal Molecular Free Volume: A Mechanism for the Simultaneous Enhancement of Polymer Stiffness, Strength, and Ductility. *Macromolecules* **2006**, *39*, 3350−3358.
(39) He, Y.; Benedetti, F. M.; Lin, S.; Liu, C.; Zhao, Y.; Ye, H.-Z.; Van Voorhis, T.; De Angelis, M. G.; Swager, T. M.; Smith, Z. P. Polymers with Side Chain Porosity for Ultrapermeable and Plasticization Resistant Materials for Gas Separations. *Adv. Mater.* **2019**, *31*, 1807871.
(40) Blanchard, L. A.; Hancu, D.; Beckman, E. J.; Brennecke, J. F. Green processing using ionic liquids and CO_2. *Nature* **1999**, *399*, 28−29.
(41) Plechkova, N. V.; Seddon, K. R. Applications of ionic liquids in the chemical industry. *Chem. Soc. Rev.* **2008**, *37*, 123−150.
(42) Tang, J.; Sun, W.; Tang, H.; Radosz, M.; Shen, Y. Enhanced CO_2 Absorption of Poly(ionic liquid)s. *Macromolecules* **2005**, *38*, 2037−2039.
(43) Earle, M. J.; Seddon, K. R. Ionic liquids. Green solvents for the future. *Pure Appl. Chem.* **2000**, *72*, 1391−1398.

https://dx.doi.org/10.1021/acs.macromol.0c01321
Macromolecules 2020, 53, 8951−8959

(44) Wasserscheid, P.; Keim, W. Ionic Liquids—New "Solutions" for Transition Metal Catalysis. *Am. Ethnol.* **2000**, *39*, 3772−3789.
(45) Morgan, D.; Ferguson, L.; Scovazzo, P. Diffusivities of Gases in Room-Temperature Ionic Liquids: Data and Correlations Obtained Using a Lag-Time Technique. *Ind. Eng. Chem. Res.* **2005**, *44*, 4815−4823.
(46) Scovazzo, P.; Kieft, J.; Finan, D. A.; Koval, C.; DuBois, D.; Noble, R. Gas separations using non-hexafluorophosphate $[PF6]^-$ anion supported ionic liquid membranes. *J. Membr. Sci.* **2004**, *238*, 57−63.
(47) Gan, Q.; Rooney, D.; Xue, M.; Thompson, G.; Zou, Y. An experimental study of gas transport and separation properties of ionic liquids supported on nanofiltration membranes. *J. Membr. Sci.* **2006**, *280*, 948−956.
(48) Ferguson, L.; Scovazzo, P. Solubility, Diffusivity, and Permeability of Gases in Phosphonium-Based Room Temperature Ionic Liquids: Data and Correlations. *Ind. Eng. Chem. Res.* **2007**, *46*, 1369−1374.
(49) Bara, J. E.; Lessmann, S.; Gabriel, C. J.; Hatakeyama, E. S.; Noble, R. D.; Gin, D. L. Synthesis and performance of polymerizable room-temperature ionic liquids as gas separation membranes. *Ind. Eng. Chem. Res.* **2007**, *46*, 5397−5404.
(50) Tang, H.; Tang, J.; Ding, S.; Radosz, M.; Shen, Y. Atom transfer radical polymerization of styrenic ionic liquid monomers and carbon dioxide absorption of the polymerized ionic liquids. *J. Polym. Sci., Part A: Polym. Chem.* **2005**, *43*, 1432−1443.
(51) Bara, J. E.; Hatakeyama, E. S.; Gin, D. L.; Noble, R. D. Improving CO_2 permeability in polymerized room-temperature ionic liquid gas separation membranes through the formation of a solid composite with a room-temperature ionic liquid. *Polym. Adv. Technol.* **2008**, *19*, 1415−1420.
(52) Tang, J.; Tang, H.; Sun, W.; Plancher, H.; Radosz, M.; Shen, Y. Poly (ionic liquid)s: a new material with enhanced and fast CO_2 absorption. *Chem. Commun.* **2005**, *26*, 3325−3327.
(53) Du, N.; Park, H. B.; Robertson, G. P.; Dal-Cin, M. M.; Visser, T.; Scoles, L.; Guiver, M. D. Polymer nanosieve membranes for CO_2-capture applications. *Nat. Mater.* **2011**, *10*, 372−375.
(54) Du, N.; Guiver, M. D. Polymers of intrinsic microporosity containing tetrazole groups. US patent 8,623,928, January 7th , 2014.
(55) Bates, E. D.; Mayton, R. D.; Ntai, I.; Davis, J. H. CO_2 Capture by a Task-Specific Ionic Liquid. *J. Am. Chem. Soc.* **2002**, *124*, 926−927.
(56) Aronson, J. B. The synthesis and characterization of energetic materials from sodium azide. Doctorate thesis, Georgia Institute of Technology, 2004. http://hdl.handle.net/1853/7597.
(57) Laas, H.-J.; Halpaap, R.; Richter, F.; Kocher, J. Ionic liquids. US patent 2003/020441, October 30th, 2003.
(58) Du, N.; Robertson, G. P.; Song, J.; Pinnau, I.; Thomas, S.; Guiver, M. D. Polymers of Intrinsic Microporosity Containing Trifluoromethyl and Phenylsulfone Groups as Materials for Membrane Gas Separation. *Macromolecules* **2008**, *41*, 9656−9662.
(59) Vygodskii, Y. S.; Mel'nik, O. A.; Kazakova, E. V.; Shaplov, A. S.; Komarova, L. I.; Kizhnyaev, V. N. Free-radical polymerization of C-vinyltetrazoles: Effect of the nature of ionic solvents. *Polymer Science Series B* **2008**, *50*, 193−197.
(60) Dişli, A.; Salman, M. Synthesis of some new 5-substituted 1H-tetrazoles. *Russ. J. Org. Chem.* **2009**, *45*, 151.
(61) Darkow, R.; Hartmann, U.; Tomaschewski, G. Synthesis, photomodification and characterization of homo- and copolymers with 2,5-bisaryltetrazolyl pendant groups. *React. Funct. Polym.* **1997**, *32*, 195−207.
(62) Du, N.; Robertson, G. P.; Dal-Cin, M. M.; Scoles, L.; Guiver, M. D. Polymers of intrinsic microporosity (PIMs) substituted with methyl tetrazole. *Polymer* **2012**, *53*, 4367−4372.
(63) Prokudin, V. G.; Poplavsky, V. S.; Ostrovskii, V. A. Mechanism of the monomolecular thermal decomposition of tetrazole and 5-substituted tetrazoles. *Russ. Chem. Bull.* **1996**, *45*, 2101−2104.
(64) Yong, W. F.; Kwek, K. H. A.; Liao, K.-S.; Chung, T.-S. Suppression of aging and plasticization in highly permeable polymers. *Polymer* **2015**, *77*, 377−386.
(65) Du, N.; Robertson, G. P.; Pinnau, I.; Guiver, M. D. Polymers of intrinsic microporosity derived from novel disulfone-based monomers. *Macromolecules* **2009**, *42*, 6023−6030.
(66) Li, F. Y.; Xiao, Y.; Ong, Y. K.; Chung, T. S. UV-rearranged PIM-1 polymeric membranes for advanced hydrogen purification and production. *Adv. Energy Mater.* **2012**, *2*, 1456−1466.
(67) Wu, X. M.; Zhang, Q. G.; Lin, P. J.; Qu, Y.; Zhu, A. M.; Liu, Q. L. Towards enhanced CO_2 selectivity of the PIM-1 membrane by blending with polyethylene glycol. *J. Membr. Sci.* **2015**, *493*, 147−155.
(68) Swaidan, R.; Ghanem, B.; Litwiller, E.; Pinnau, I. Physical aging, plasticization and their effects on gas permeation in "rigid" polymers of intrinsic microporosity. *Macromolecules* **2015**, *48*, 6553−6561.
(69) Bezzu, C. G.; Carta, M.; Ferrari, M.-C.; Jansen, J. C.; Monteleone, M.; Esposito, E.; Fuoco, A.; Hart, K.; Liyana-Arachchi, T. P.; Colina, C. M.; McKeown, N. B. The synthesis, chain-packing simulation and long-term gas permeability of highly selective spirobifluorene-based polymers of intrinsic microporosity. *J. Mater. Chem. A* **2018**, *6*, 10507−10514.
(70) Short, R.; Carta, M.; Bezzu, C. G.; Fritsch, D.; Kariuki, B. M.; McKeown, N. B. Hexaphenylbenzene-based polymers of intrinsic microporosity. *Chem. Commun.* **2011**, *47*, 6822−6824.
(71) Carta, M.; Bernardo, P.; Clarizia, G.; Jansen, J. C.; McKeown, N. B. Gas permeability of hexaphenylbenzene based polymers of intrinsic microporosity. *Macromolecules* **2014**, *47*, 8320−8327.
(72) Ma, X.; Pinnau, I. A novel intrinsically microporous ladder polymer and copolymers derived from 1, 1′, 2, 2′-tetrahydroxy-tetraphenylethylene for membrane-based gas separation. *Polym. Chem.* **2016**, *7*, 1244−1248.
(73) Zhang, J.; Kang, H.; Martin, J.; Zhang, S.; Thomas, S.; Merkel, T. C.; Jin, J. The enhancement of chain rigidity and gas transport performance of polymers of intrinsic microporosity via intramolecular locking of the spiro-carbon. *Chem. Commun.* **2016**, *52*, 6553−6556.
(74) Ghanem, B.; Alghunaimi, F.; Alaslai, N.; Ma, X.; Pinnau, I. New phenazine-containing ladder polymer of intrinsic microporosity from a spirobisindane-based AB-type monomer. *RSC Adv.* **2016**, *6*, 79625−79630.
(75) Carta, M.; Croad, M.; Jansen, J. C.; Bernardo, P.; Clarizia, G.; McKeown, N. B. Synthesis of cardo-polymers using Tröger's base formation. *Polym. Chem.* **2014**, *5*, 5255−5261.
(76) Williams, R.; Burt, L. A.; Esposito, E.; Jansen, J. C.; Tocci, E.; Rizzuto, C.; Lanč, M.; Carta, M.; McKeown, N. B. A highly rigid and gas selective methanopentacene-based polymer of intrinsic microporosity derived from Tröger's base polymerization. *J. Mater. Chem. A* **2018**, *6*, 5661−5667.
(77) Robeson, L. M. Correlation of separation factor versus permeability for polymeric membranes. *J. Membr. Sci.* **1991**, *62*, 165−185.
(78) Robeson, L. M. The upper bound revisited. *J. Membr. Sci.* **2008**, *320*, 390−400.
(79) Swaidan, R.; Ghanem, B.; Pinnau, I. Fine-Tuned Intrinsically Ultramicroporous Polymers Redefine the Permeability/Selectivity Upper Bounds of Membrane-Based Air and Hydrogen Separations. *ACS Macro Lett.* **2015**, *4*, 947−951.
(80) Comesaña-Gándara, B.; Chen, J.; Bezzu, C. G.; Carta, M.; Rose, I.; Ferrari, M.-C.; Esposito, E.; Fuoco, A.; Jansen, J. C.; McKeown, N. B. Redefining the Robeson upper bounds for CO_2/CH_4 and CO_2/N_2 separations using a series of ultrapermeable benzotriptycene-based polymers of intrinsic microporosity. *Energy Environ. Sci.* **2019**, *12*, 2733−2740.

https://dx.doi.org/10.1021/acs.macromol.0c01321
Macromolecules 2020, 53, 8951−8959